1 **TITLE**

2 Amazon forest response to CO_2 fertilization dependent on plant phosphorus acquisition

3 **AUTHORS AFFILITATIONS**

4 Katrin Fleischer*, *Land Surface–Atmosphere Interactions, Technical University of Munich,*

5 *Germany*

6 Anja Rammig, *Land Surface–Atmosphere Interactions, Technical University of Munich,*

7 *Germany*

8 Martin G. De Kauwe[1,2], [1]*Climate Change Research Centre, University of New South Wales,*

9 *Sydney, NSW 2052, Australia;* [2]*ARC Centre of Excellence for Climate Extremes, Sydney, NSW*

10 *2052, Australia*

11 Anthony P. Walker, *Environmental Sciences Division and Climate Change Science Institute,*

12 *Oak Ridge National Laboratory, Oak Ridge, TN, USA*

13 Tomas F. Domingues, *FFCLRP, Department of Biology, University of São Paulo, Brazil*

14 Lucia Fuchslueger[1,2], [1]*National Institute of Amazonian Research (INPA), Brazil;* [2]*University*

15 *of Antwerp, Belgium*

16 Sabrina Garcia, *National Institute of Amazonian Research (INPA), Brazil*

17 Daniel S. Goll[1,2], [1]*Laboratoire des Sciences du Climat et de l'Environnement, LSCE/IPSL,*

18 *CEA–CNRS–UVSQ, France;* [2]*Lehrstuhl für Physische Geographie mit Schwerpunkt*

19 *Klimaforschung, Universität Augsburg, Alter Postweg 118, D-86135 Augsburg, Germany*

20 Adriana Grandis, *University of São Paulo, Brazil*

21 Mingkai Jiang, *Hawkesbury Institute for the Environment, Western Sydney University,*

22 *Australia*

23 Vanessa Haverd, *CSIRO Oceans and Atmosphere, Canberra, 2601, Australia*

24 Florian Hofhansl, *International Institute for Applied Systems Analysis, Schlossplatz 1, A-2361*

25 *Laxenburg, Austria*

26 Jennifer A. Holm, *Lawrence Berkeley National Laboratory, Berkeley, California, United*

27 *States*

28 Bart Kruijt, *Alterra Wageningen, The Netherlands*

29 Felix Leung[1,2], [1]*College of Life and Environmental Sciences, University of Exeter, EX4 4QE,*

30 *UK;* [2]*Institute of Environment, Energy and Sustainability, The Chinese University of Hong*

31 *Kong, Hong Kong*

32 Belinda E. Medlyn, *Hawkesbury Institute for the Environment, Western Sydney University,*

33 *Australia*

34 Lina M. Mercado[1,2], *[1]College of Life and Environmental Sciences, University of Exeter, EX4*

35 *4QE, UK; [2]Centre for Ecology and Hydrology, Wallingford, OX10 8BB, UK*

36 Richard J. Norby, *Environmental Sciences Division and Climate Change Science Institute,*

37 *Oak Ridge National Laboratory, Oak Ridge, TN, USA*

38 Bernard Pak, *CSIRO Oceans and Atmosphere, Aspendale Victoria 3195, Australia*

39 Carlos A. Quesada, *National Institute of Amazonian Research (INPA), Brazil*

40 Celso von Randow, *National Institute for Space Research (INPE), Brazil*

41 Karst J. Schaap, *National Institute of Amazonian Research (INPA), Brazil*

42 Oscar J. Valverde-Barrantes, *International Center of Tropical Botany, Florida International*

43 *University, United States*

44 Ying-Ping Wang, *CSIRO Oceans and Atmosphere, Aspendale Victoria 3195, Australia*

45 Xiaojuan Yang, *Environmental Sciences Division and Climate Change Science Institute, Oak*

46 *Ridge National Laboratory, Oak Ridge, TN, USA*

47 Sönke Zaehle, *Max-Planck Institute for Biogeochemistry, Germany*

48 Qing Zhu, *Lawrence Berkeley National Laboratory, Berkeley, California, United States*

49 David M. Lapola, *Center for Meteorological and Climatic Research Applied to Agriculture,*

50 *University of Campinas, Brazil*

51 *corresponding author

52 **MAIN TEXT**

53 **Global terrestrial models currently predict that the Amazon rainforest will continue to**

54 **act as a carbon sink in the future primarily due to the rising atmospheric carbon dioxide**

55 **(CO_2) concentration. Soil phosphorus impoverishment in parts of the Amazon basin**

56 **largely controls its functioning, but the role of phosphorus availability has not been**

57 **considered in global model ensembles, e.g., during the 5th Climate Model**

58 **Intercomparison Project (CMIP5). Here, we simulate the planned free-air CO_2**

59 **enrichment experiment AmazonFACE with an ensemble of 14 terrestrial ecosystem**

60 **models. We show that phosphorus availability reduces the projected CO_2-induced**

61 **biomass carbon growth by about 50% to 79 ± 63 g C m^{-2} yr^{-1} over 15 years compared to**

62 **estimates from carbon and carbon-nitrogen models. Our results suggest that the**

63 **region's resilience to climate change may be much less than previously assumed.**

64 **Variation in the biomass carbon response among the phosphorus-enabled models is**

65 **considerable, ranging from 5 to 140 g C m^{-2} yr^{-1}, due to contrasting plant phosphorus**

66 **use and acquisition strategies considered among the models. The Amazon forest**

67 **response will thus depend on the interactions and relative contributions of the**

68 **phosphorus acquisition and use strategies across individuals, and to what extent these**

69 **processes can be upregulated under eCO_2.**

70 The intact Amazon rainforest acts as a substantial carbon (C) sink, completely offsetting

71 carbon dioxide (CO_2) emissions from fossil fuel combustion and land use change in the

72 Amazon region[1,2]. Increasing atmospheric CO_2 concentrations from anthropogenic activity

73 may be the primary factor for the current Amazon net C sink[1,3], via so-called CO_2 fertilization

74 (an increase in photosynthetic C uptake by plants under higher CO_2), which is projected to

75 continue into the future by global models[4-6]. The CO_2 fertilization effect has been observed

76 experimentally in field experiments that were conducted predominantly in the temperate zone.

77 In these experiments, the eCO$_2$ induced increase in C uptake was generally low when other

78 factors, such as soil nitrogen (N), were limiting[7–9]. To date, whole-ecosystem-scale

79 experiments, i.e., free-air CO$_2$ enrichment (FACE) have never been conducted in the

80 tropics[10,11].

81 Over large parts of the Amazon and the tropics worldwide, phosphorus (P), not N, is assumed

82 to be the key limiting nutrient, as most P has been lost or occluded from plant uptake during

83 millions of years of soil pedogenesis[12,13]. Forests growing on these highly weathered old soils

84 may nonetheless be highly productive due to the evolution of multiple strategies for P

85 acquisition and use, enabling tight cycling of P between plants and soils[14,15]. Despite this

86 knowledge, quantifying the control of P on plant physiology, growth, and plant-soil

87 interactions in global models, and hence its role in the forests' response to eCO$_2$, remains

88 challenging[16,17]. This challenge is exacerbated by the scarcity of observations and distinctive

89 species responses in hyperdiverse tropical forests[18].

90 **Predicted nutrient feedbacks to eCO$_2$ at the AmazonFACE site**

91 Here, we study the potential interactions between eCO$_2$ and nutrient (N and P) feedbacks in a

92 mature Amazonian rainforest by simulating the planned AmazonFACE experiment (+200

93 ppm; https://amazonface.inpa.gov.br/) with an ensemble of ecosystem models (n = 14,

94 Extended Data Table 3), including three C, five carbon-nitrogen (CN), and six carbon-

95 nitrogen-phosphorus (CNP) models[19–24]. The AmazonFACE experiment is located in a well-

96 studied, highly productive tropical forest in Central Amazonia[25,26], growing on a strongly

97 weathered *terra firme* Ferralsol. This ecosystem represents the low end of the plant-available

98 P spectrum in the Amazon, consistent with ~32% of the Amazon rainforest's cover fraction[27].

99 *In situ* measurements were used to parameterise the models and to evaluate simulated ambient

100 conditions (Extended Data Table 1, 2). Our aim was to generate *a priori* model-based

101 hypotheses to highlight the state-of-the-knowledge and guide measurement strategies for

102 AmazonFACE and other ecosystem manipulation experiments to gain crucial process

103 understanding of P control on the CO_2 fertilization effect.

104 Simulated eCO_2 (+200 ppm) had a positive effect on plant biomass C across all models but

105 was weakest in the CNP models (Fig. 1a). The eCO_2 conditions induced average biomass C

106 gains of 163 ± 65, 145 ± 83, and 79 ± 63 g C m^{-2} yr^{-1} (mean $\pm$ SD) over 15 years in the C, CN

107 and CNP models, respectively (Fig. 1a). Limitations by P thus reduced the predicted biomass

108 C sink by 52% and 46% compared to that in the C and CN models, respectively, with

109 considerable variation across and within model groups (Extended Data Fig. 1). Plot

110 inventories at the AmazonFACE site during the 2000s indicate an aboveground biomass

111 increment of 23 g C m^2 yr^{-1}, substantially below the Amazon-wide[1] estimate of 64 g C m^2 yr^{-1}.

112 The model ensemble represents ambient conditions, such as productivity and leaf area index,

113 reasonably well, but ensemble members show divergence in other ecosystem characteristics,

114 such as the biomass C increment, which range from 5 to 114 g C m^2 yr^{-1}. There is, however,

115 no clear pattern in performance between the model groups, so that we judge that these

116 differences do not have bearing on the conclusions of our study (see more discussion in

117 Extended Data Fig. 2).

Differing model responses to phosphorus limitation

119 Gross and net primary productivity (GPP and NPP, respectively) are both stimulated by eCO_2

120 in all models, both initially (after 1 year of eCO_2) and until the end of the simulation. The

121 CNP models show the strongest decline from the initial response due to P limitation (Fig. 1b,

122 c). The final response of NPP to eCO_2 was a 35%, 29%, and 9% stimulation for the C, CN

123 and CNP models, respectively. In general, in the CN and CNP models, nutrient limitation is

124 defined as nutrient demand being greater than nutrient supply. However, models differ in their

125 assumptions on how nutrient limitation controls productivity and C allocation in response to

126 eCO_2, so that divergent responses on plant carbon use efficiency (CUE = NPP / GPP) are

127   simulated (Extended Data Table 3). In some CN models, CUE increases because N limitation

128   is hypothesized to reduce autotrophic respiration (Ra) via lower tissue N content. Some CNP

129   models, however, assume a direct downregulation of growth and hence the plant CUE

130   decreases (Extended Data Fig. 3). Elevated CO_2 induced higher fine root investments of NPP

131   in some CN and CNP models to aid nutrient acquisition (Fig. 1c; Extended Data Fig. 4).

132   Predicted changes in allocation with eCO_2 cause a general increase in biomass turnover across

133   all but one of the models, partially offsetting the positive biomass response (Extended Data

134   Table 4). Changes in turnover play a minor role in our 15 years simulation period but rather

135   control the long-term future CO_2 effect on the biomass C sink[28,29].

136   Plant growth under eCO_2 is lowest in CNP models as the low availability of soil labile P

137   restricts P uptake either immediately or over time (Extended Data Fig. 5). We considered the

138   modelled P limitation on plant growth to be realistic, as the models and observations agree on

139   soil labile P being very low (Extended Data Fig. 2). Other site observations support the fact

140   that P is extremely critical for plant productivity, such as high leaf N:P ratios of 37 and high

141   plant P resorption (before litter fall) of 78% (Extended Data Table 1). While P limitation

142   consistently reduces the eCO_2-induced biomass C sink, there is significant variation among

143   CNP models due to contrasting process representations (Fig. 2; Extended Data Table 3). P

144   shortages downregulate growth (i.e., NPP) in all CNP models, directly or via photosynthesis.

145   The major differences in the model assumptions relate to how they modify P supply and

146   demand to alleviate plant P shortages, including either (i) enhancing plant P use efficiency

147   (PUE = NPP / P uptake) or (ii) upregulating P acquisition mechanisms. The models assume

148   that PUE may change if tissue nutrient ratios are flexible, if C allocation changes among

149   tissues with different stoichiometry, and/or if P resorption is variable (Fig. 2). Flexible

150   stoichiometry is considered in all CNP models except ELM-CTC, although with varying

151   degrees of flexibility. Greater fine root C allocation with plant P stress is considered in some,

152   and P resorption is a fixed fraction of leaf tissue P in all models (Fig. 2).

153   Models differ in their representation of soil P acquisition mechanisms; three of the six models

154   (ELM-ECA, ELM-CTC, GDAY) consider desorption of P from mineral surfaces (i.e., the

155   secondary or strongly sorbed P pool), whereas the others assume P in those pools to be

156   unavailable to plants. All the models include biochemical mineralization of organic P via

157   phosphatase, but only three (ELM-ECA, ELM-CTC and ORCHIDEE) include the

158   functionality to increase P acquisition via this mechanism under plant P stress (Fig. 2;

159   Extended Data Table 3). Litter and soil stoichiometry are considered with varying degrees of

160   flexibility. Soil labile P limits microbial decomposition rates of litter and soil, so that

161   decomposition is reduced when immobilization demands for P exceed soil labile P availability

162   (Fig. 2; Extended Data Table 3).

163   **Enhanced phosphorus use efficiency and acquisition due to eCO_2**

164   Diverging representations of plant P use and acquisition among the CNP models cause

165   predictions of the eCO_2-induced biomass C sink to range from 5 g C m^{-2} yr^{-1} to 140 g C m^{-2}

166   yr^{-1} (Fig. 3a; Extended Data Fig. 1). Greater plant PUE occurred in four of the models, for

167   which shifts in tissue C:N and N:P due to eCO_2 led to increases in biomass C:P ranging from

168   ~200 to 1600 g C g P^{-1} (Fig. 3c). Higher fine root investment with eCO_2, at the expense of less

169   "P-costly" wood, offset some increases in PUE in some models. Flexible biomass

170   stoichiometry altered decomposition dynamics and induced progressive P limitation in

171   response to eCO_2, i.e., litter stoichiometry shifted towards lower quality (less N and P in

172   relation to C), reducing net P mineralization rates from microbial decomposition, causing P to

173   become increasingly unavailable to plants and accumulating in soil organic matter (Fig. 3d, e).

174   This plant-soil-microbial feedback slowed the cycling of P in the ecosystem and exacerbated

175   the initial P limitation (see Ref. [30] for a similar feedback during pedogenesis).

176 Enhanced plant P acquisition under eCO_2 effectively alleviated P limitation in two CNP

177 models (ELM-CTC and ELM-ECA) (Fig. 3e). In both, eCO_2 increased the liberation of P

178 from the secondary pool, as higher plant P demand and uptake diminished the labile P pool, in

179 turn causing higher desorption rates. P desorption is thus only indirectly, and not

180 mechanistically, enhanced by plants in these models. Biochemical mineralization of P under

181 eCO_2 responded positively in both of the models, but added only notably to additional P

182 acquisition in ELM-CTC (Fig. 3e). Although three CNP models simulated higher fine root

183 investments, the actual P uptake return per fine root increment was marginal or came only into

184 effect in the long-term (Extended Data Fig. 6).

185 Observations document ample N cycling in the system, e.g., high leaf N contents, indicative

186 $\delta^{15}N$ values, high rates of N oxide emissions, and low leaf N resorption[31,32], and thereby

187 suggest that plant growth is not directly affected by N availability. The CN models, however,

188 simulate increased nitrogen use efficiency (NUE) and biomass C:N ratios, in response to

189 insufficient N uptake under eCO_2 (Extended Data Fig. 5). Plant N availability may be

190 underestimated in the models, since the plant-available mineral N supply was <7 g N m^{-2}

191 across all models, as opposed to 17.5 g N m^{-2} observed in the top 10 cm only (Extended Data

192 Fig. 2). These results highlight an important gap in our knowledge also related to the

193 dynamics of N availability, and its potential interaction with P dynamics (Table 1).

194 **Model-based hypotheses for the AmazonFACE experiment**

195 In summary, the model ensemble encapsulates a range of plausible hypotheses and represents

196 a potential range of biomass C responses to eCO_2 under low soil P availability. The

197 assumption of a lacking ability of plants to acquire more soil P and a limited capacity for

198 plants to use P more efficiently resulted in effectively zero biomass C gain with eCO_2.

199 Conversely, flexible stoichiometry, in combination with enhanced plant P acquisition, were

200 the key mechanistic responses leading to biomass gain with eCO_2. Divergences in the

201 simulated eCO_2 response lead us to the following testable hypotheses, and call for directed

202 field measurements (Table 1):

203 H1. Low soil P availability will strongly constrain future plant biomass growth response to

204 eCO_2 either by downregulating photosynthesis or limiting plant growth directly, or a

205 combination thereof.

206 H2. Despite the limited soil P supply, plasticity in vegetation stoichiometry and allocation

207 patterns will allow for some biomass growth under eCO_2.

208 H3. Plants will increase investments in P acquisition to increase P supply and allow biomass

209 growth under eCO_2 either via greater P interception through fine root production or via greater

210 P liberation from P desorption or biochemical mineralization of P.

211 These model-based hypotheses deepen a previous analysis of potential N and P limitation on

212 C accumulation based on mass balance principle[33]. Furthermore, we add to a model

213 intercomparison carried out in advance of the EucFACE experiment[34] by extending the range

214 of plant P feedbacks considered across CNP models. This work highlighted H1: two

215 stoichiometrically constrained CNP models predicted that strong P limitation will curtail the

216 growth response to eCO_2 in Australia. Consistent with this hypothesis, aboveground growth

217 has not increased with eCO_2 in that experiment over the initial years[35]. This finding underlines

218 that monitoring efforts need to place a strong(er) focus on belowground carbon and nutrient

219 dynamics, in addition to canopy-scale photosynthesis and aboveground growth dynamics.

220 Additionally, Ra dependence on P content and plant stress from drought or nutrient limitation

221 need further monitoring during experiments to fully elucidate the plant C budget and address

222 H1 (Table 1).

223 Nutrient fertilization experiments support H2, as plasticity in leaf stoichiometry at the

224 individual level, along with plasticity in P resorption efficiency, was observed[36]. Across the

225   Amazon, community-weighted leaf N:P in the field varied from 13 to 42 g N g P^{-1} (n = 64)

226   (Ref. [32]), which place our site, with a mean of 37, closer to the high end. GDAY predicted the

227   most plausible increase in the leaf N:P ratio from 34 to 38 (Extended Data Fig. 7). Two

228   models predicted strong increases in the leaf N:P ratio with eCO_2 but started off with much

229   lower initial values. The degree to which plasticity in stoichiometry and resorption can aid

230   plant PUE under eCO_2 in highly P-limited sites that are already at the end of the observed

231   spectrum remains to be seen (H2). Monitoring plant tissue stoichiometry, including wood

232   with much higher N:P ratios, combined with assessments of P resorption in CO_2 and nutrient

233   fertilization experiments will reduce uncertainties (Table 1).

234   Based on previous observations[8], a number of models assume increased fine root investment,

235   as well as higher biochemical P mineralization and P desorption from mineral surfaces, under

236   eCO_2-induced nutrient limitation (H3). The effect of increased fine root biomass on nutrient

237   uptake was limited in our simulations and ambient fine root allocation fractions were highly

238   variable among the models, ranging from 5-30% of NPP (Extended Data Fig. 4, 6). Both these

239   modelled results highlight model deficiencies in belowground processes[37] that need

240   addressing (Table 1). There is evidence that phosphatase activity in litter and soil and the

241   presence of low-molecular-weight acids used to liberate P from organic matter or from

242   mineral surfaces increase with plant P demand[38]. This was predicted by ELM-CTC in our

243   simulations, which also showed Amazon-wide that "[with] enhanced phosphatase production,

244   productivity in the highly P-limited areas can be sustained under elevated CO_2 conditions"[39].

245   Plants invest in P liberation and acquisition, but if these mechanisms can be upregulated under

246   eCO_2 and over what time frame this may occur remain open questions. Quantification of such

247   a response is lacking, as are estimates of the associated plant C costs to acquire P via these

248   and other mechanisms, such as mycorrhizal symbiosis[15,40] (Table 1). The P gain and C cost

249   for P acquisition mechanisms, as well as the associated plant-soil-microbial interactions, need

250 to be assessed by analyses of soil, microbial and root nutrition, and via novel techniques

251 investigating enzyme and labile C dynamics[41]. Monitoring of belowground fine root dynamics

252 needs to include the surface litter layer, commonly explored by fine roots in P-impoverished

253 ecosystems in the Amazon, not yet quantified nor considered in models (Table 1).

254 **Implications of considering phosphorus for the CO_2 fertilization effect**

255 Previous model projections suggest a sustained fertilization effect of CO_2 on the Amazon C

256 sink but have not considered feedbacks from low soil P availability[5,6]. Our study demonstrates

257 that, based on the current generation of CNP models, the omission of P feedbacks is highly

258 likely to cause an overestimation of the Amazon rainforest's capacity to sequester

259 atmospheric CO_2. Considering P limitation on the CO_2 fertilization effect in future predictions

260 may indicate that the forest is less resilient to higher temperatures and changing rainfall

261 patterns than previously thought[6,42]. Periods of water deficit may contribute to the eCO_2

262 fertilization effect on productivity due to its water saving effect[34], or due to alterations of

263 decomposition processes. Our study site experienced years with significantly less than

264 average precipitation, e.g. in 2000 and 2009, however, in our simulations this increased the

265 positive response of GPP and NPP to eCO_2 only marginally (Extended Data Figure 8 and 9).

266 Models lack the appropriate sensitivity of plant responses to changes in water availability, and

267 even more so when precipitation sums are that high[43]. Interactions of water and P availability

268 and their consequences on the CO_2 fertilization effect remain uncertain[44] and is an area where

269 field measurements will allow us to better constrain model responses (Table 1).

270 Although P is likely to reduce the biomass C sink response to CO_2 in regions with low plant-

271 available P supply, our results suggest that plasticity in plant P use and plant P acquisition

272 mechanisms, may at least partially alleviate P limitation under eCO_2 and enable CO_2

273 fertilization of biomass growth. The model ensemble may be interpreted as representing a

274 range of possible tropical plant functional strategies and growth responses to low P

275 availability under eCO_2. Responses are expected to be species-specific, as were plant growth

276 responses to low P supplies in another tropical region[18]. The ecosystem-scale response to P

277 limitation under eCO_2 will thus depend on the relative contributions of the various P

278 acquisition and P use strategies across individuals, their interactions and to what extent these

279 processes can be upregulated under eCO_2. All of which ultimately need to be described and

280 represented in a single model framework in order to accurately predict the Amazon

281 rainforest's response to future climate change.

282 AmazonFACE has the unique opportunity to experimentally address these key areas of

283 uncertainty, not only by integrating the proposed measurements across seasons and at the

284 ecosystem scale (summary in Table 1) but also by assessing species-specific responses to

285 eCO_2 in relation to trait expression. Amazon-wide expression of plant functional strategies

286 may then be inferred by applying the mechanistic interplay between trait expression and

287 edaphic conditions. The key to predicting the future of the world's largest tropical forest

288 under eCO_2 thus lies in obtaining experimental data on, and subsequently modelling, different

289 plant P acquisition and use strategies, as well as their interactions in a competing plant

290 community.

REFERENCES

291

292   1.   Brienen, R. J. W. *et al.* Long-term decline of the Amazon carbon sink. *Nature* **519,**

293   344–348 (2015).

294   2.   Phillips, O. L. & Brienen, R. J. W. Carbon uptake by mature Amazon forests has

295   mitigated Amazon nations' carbon emissions. *Carbon Balance Manag.* **12,** 1 (2017).

296   3.   Cernusak, L. A. *et al.* Tropical forest responses to increasing atmospheric CO2: Current

297   knowledge and opportunities for future research. *Funct. Plant Biol.* **40,** 531–551

298   (2013).

299   4.   Ciais, P. *et al.* The physical science basis. Contribution of working group I to the fifth

300   assessment report of the intergovernmental panel on climate change. *Chang. IPCC*

301   *Clim.* 465–570 (2013).

302   5.   Cox, P. M. *et al.* Sensitivity of tropical carbon to climate change constrained by carbon

303   dioxide variability. *Nature* **494,** 341–344 (2013).

304   6.   Huntingford, C. *et al.* Simulated resilience of tropical rainforests to CO_2-induced

305   climate change. *Nat. Geosci.* **6,** 268–273 (2013).

306   7.   Talhelm, A. F. *et al.* Elevated carbon dioxide and ozone alter productivity and

307   ecosystem carbon content in northern temperate forests. *Glob. Chang. Biol.* **20,** 2492–

308   2504 (2014).

309   8.   Norby, R. J., Warren, J. M., Iversen, C. M., Medlyn, B. E. & McMurtrie, R. E. CO2

310   enhancement of forest productivity constrained by limited nitrogen availability. *Proc.*

311   *Natl. Acad. Sci.* **107,** 19368–19373 (2010).

312   9.   Zaehle, S. *et al.* Evaluation of 11 terrestrial carbon-nitrogen cycle models against

313   observations from two temperate Free-Air CO2Enrichment studies. *New Phytol.* **202,**

314   803–822 (2014).

315   10.   Hofhansl, F. *et al.* Amazon forest ecosystem responses to elevated atmospheric CO2

316   and alterations in nutrient availability: filling the gaps with model-experiment

317   integration. *Front. Earth Sci.* **4,** (2016).

318   11.   Norby, R. J. *et al.* Model-data synthesis for the next generation of forest free-air CO2

319   enrichment (FACE) experiments. *New Phytol.* **209,** 17–28 (2016).

320   12.   Lloyd, J., Bird, M. I., Veenendaal, E. M. & Kruijt, B. Should Phosphorus Availability

321   Be Constraining Moist Tropical Forest Responses to Increasing CO2 Concentrations?

322   *Glob. Biogeochem. Cycles Clim. Syst.* 95–114 (2001).

323   13.   Vitousek, P. M. Litterfall, nutrient cycling, and nutrient limitation in tropical forests.

324   *Ecology* **65,** 285–298 (1984).

325   14.   Quesada, C. A. *et al.* Basin-wide variations in Amazon forest structure and function are

326   mediated by both soils and climate. *Biogeosciences* **9,** 2203–2246 (2012).

327   15.   Lambers, H., Raven, J. A., Shaver, G. R. & Smith, S. E. Plant nutrient-acquisition

328   strategies change with soil age. *Trends Ecol. Evol.* **23,** 95–103 (2008).

329   16.   Reed, S. C., Yang, X. & Thornton, P. E. Incorporating phosphorus cycling into global

330   modeling efforts: A worthwhile, tractable endeavor. *New Phytol.* **208,** 324–329 (2015).

331   17.   Jiang, M., Caldararu, S., Zaehle, S., Ellsworth, D. S. & Medlyn, B. E. Towards a more

332   physiological representation of vegetation phosphorus processes in land surface

333   models. *New Phytol.* 1–7 (2019).

334   18.   Turner, B. L., Brenes-Arguedas, T. & Condit, R. Pervasive phosphorus limitation of

335   tree species but not communities in tropical forests. *Nature* **555,** 367–370 (2018).

336   19.   Goll, D. S. *et al.* A representation of the phosphorus cycle for ORCHIDEE (revision

337   4520). *Geosci. Model Dev.* **10,** 3745–3770 (2017).

338 20. Wang, Y.-P., Law, R. M. & Pak, B. A global model of carbon, nitrogen and

339   phosphorus cycles for the terrestrial biosphere. *Biogeosciences* **7,** 2261–2282 (2010).

340 21. Haverd, V. *et al.* A new version of the CABLE land surface model (Subversion

341   revision r4601) incorporating land use and land cover change, woody vegetation

342   demography, and a novel optimisation-based approach to plant coordination of

343   photosynthesis. *Geosci. Model Dev.* **11,** 2995–3026 (2018).

344 22. Comins, H. N. & McMurtrie, R. E. Long-Term Response of Nutrient-Limited Forests

345   to CO2 Enrichment; Equilibrium Behavior of Plant-Soil Models. *Ecol. Appl.* **3,** 666–

346   681 (1993).

347 23. Zhu, Q., Riley, W. J., Tang, J. & Koven, C. D. Multiple soil nutrient competition

348   between plants, microbes, and mineral surfaces: model development, parameterization,

349   and example applications in several tropical forests. *Biogeosciences* **13,** 341–363

350   (2016).

351 24. Yang, X., Thornton, P. E., Ricciuto, D. M. & Post, W. M. The role of phosphorus

352   dynamics in tropical forests – a modeling study using CLM-CNP. *Biogeosciences* **11,**

353   1667–1681 (2014).

354 25. Malhi, Y. *et al.* Comprehensive assessment of carbon productivity, allocation and

355   storage in three Amazonian forests. *Glob. Chang. Biol.* **15,** 1255–1274 (2009).

356 26. Araújo, A. C. *et al.* Comparative measurements of carbon dioxide fluxes from two

357   nearby towers in a central Amazonian rainforest: The Manaus LBA site. *J. Geophys.*

358   *Res.* **107,** 8090 (2002).

359 27. Quesada, C. A. *et al.* Soils of Amazonia with particular reference to the RAINFOR

360   sites. *Biogeosciences* **8,** 1415–1440 (2011).

361   28.   Friend, A. D. *et al.* Carbon residence time dominates uncertainty in terrestrial

362   vegetation responses to future climate and atmospheric CO_2. *Proc. Natl. Acad. Sci.*

363   **111,** 3280–3285 (2014).

364   29.   Walker, A. P. *et al.* Predicting long-term carbon sequestration in response to CO2

365   enrichment: How and why do current ecosystem models differ? *Global Biogeochem.*

366   *Cycles* **29,** 476–495 (2015).

367   30.   Vitousek, P. M. *Nutrient cycling and limitation: Hawai'i as a model system. Princeton*

368   *University Press* (2004).

369   31.   Nardoto, G. B. *et al.* Basin-wide variations in Amazon forest nitrogen-cycling

370   characteristics as inferred from plant and soil 15N:14N measurements. *Plant Ecol.*

371   *Divers.* **7,** 173–187 (2014).

372   32.   Fyllas, N. M. *et al.* Basin-wide variations in foliar properties of Amazonian forest:

373   phylogeny, soils and climate. *Biogeosciences* **6,** 2677–2708 (2009).

374   33.   Wieder, W. R., Cleveland, C. C., Smith, W. K. & Todd-Brown, K. Future productivity

375   and carbon storage limited by terrestrial nutrient availability. *Nat. Geosci.* **8,** 441–444

376   (2015).

377   34.   Medlyn, B. E. *et al.* Using models to guide field experiments: a priori predictions for

378   the CO2 response of a nutrient- and water-limited native Eucalypt woodland. *Glob.*

379   *Chang. Biol.* **22,** 2834–2851 (2016).

380   35.   Ellsworth, D. S. *et al.* Elevated CO2 does not increase eucalypt forest productivity on a

381   low-phosphorus soil. *Nat. Clim. Chang.* **7,** 279–282 (2017).

382   36.   Wright, S. J. *et al.* Plant responses to fertilization experiments in lowland, species-rich,

383   tropical forests. *Ecology* **99,** 1129–1138 (2018).

384 37. Warren, J. M. *et al.* Root structural and functional dynamics in terrestrial biosphere

385   models--evaluation and recommendations. *New Phytol.* **205,** 59–78 (2015).

386 38. Hoosbeek, M. R. Elevated CO2 increased phosphorous loss from decomposing litter

387   and soil organic matter at two FACE experiments with trees. *Biogeochemistry* **127,** 89–

388   97 (2016).

389 39. Yang, X., Thornton, P. E., Ricciuto, D. M. & Hoffman, F. M. Phosphorus feedbacks

390   constraining tropical ecosystem responses to changes in atmospheric CO2 and climate.

391   *Geophys. Res. Lett. Res.* 7205–7214 (2016).

392 40. Vicca, S. *et al.* Fertile forests produce biomass more efficiently. *Ecol. Lett.* **15,** 520–

393   526 (2012).

394 41. Wang, Y. & Lambers, H. Root-released organic anions in response to low phosphorus

395   availability: recent progress, challenges and future perspectives. *Plant Soil* (2019).

396   doi:10.1007/s11104-019-03972-8

397 42. Gatti, L. V. *et al.* Drought sensitivity of Amazonian carbon balance revealed by

398   atmospheric measurements. *Nature* **506,** (2014).

399 43. Powell, T. L. *et al.* Confronting model predictions of carbon fluxes with measurements

400   of Amazon forests subjected to experimental drought. *New Phytol.* **200,** 350–365

401   (2013).

402 44. He, M. & Dijkstra, F. A. Drought effect on plant nitrogen and phosphorus: A meta-

403   analysis. *New Phytol.* **204,** 924–931 (2014).

404

AUTHOR CONTRIBUTIONS

DML, AR, and KF conceived the study. LF, SG, AG, FH, RN, CAQ, KJS, and OJV-B collected field data. KF, DG, MDK, MJ, VH, JAH, FL, LMM, BP, CvR, Y-PW, XY, SZ, and QZ performed model simulations. KF wrote the manuscript with contributions from all co-authors.

COMPETING INTERESTS

The authors declare no financial or non-financial competing interests.

ADDITIONAL INFORMATION

Site data used for model evaluation and calibration are available in the Supplementary Information. Model driving data can be obtained upon request by CvR. Correspondence and request for material should be addressed to KF (katrin.fleischer@tum.de).

FIGURE CAPTIONS

443 **Figure 1. The predicted effect of eCO$_2$ on biomass C, productivity and biomass**

444 **compartments for C, CN and CNP models.** (a), The final response of biomass growth,

445 calculated as the mean annual response over 15 years of eCO$_2$ in g C m^{-2} yr^{-1}. (b), first-year

446 response of productivity (GPP and NPP), and CUE (=NPP/GPP) in %. c), 15-year response of

447 productivity, CUE, and leaf, fine root and wood C (calculated as mean response of 13th to 17th

448 year), all in %. Responses to eCO$_2$ are the differences between the elevated and ambient

449 model run, shown as mean and standard deviation per model group, and individual model

450 results as dots.

451 **Figure 2. Strength of phosphorus feedbacks in controlling the biomass C response to**

452 **eCO$_2$ for the six CNP models.** The degree to which modelled P feedback on ecosystem

453 processes control the response of biomass C to eCO$_2$ in our simulations (none, intermediate,

454 high). P limitation downregulates photosynthesis or growth under eCO$_2$ in all models.

455 Maintenance respiration, leaf turnover and P resorption are not responsive to P feedbacks in

456 any of the models. Leaf N:P responds to eCO$_2$ in most models. Desorption of P from mineral

457 surfaces is only considered in ELM-ECA and ELM-CTC, and biochemical P mineralization is

458 considered in many models, but effectively responsive only in ELM-CTC. See also Extended

459 Data Table 3.

460 **Figure 3. Key responses of biomass C gain, stoichiometry, allocation, and P dynamics to**

461 **eCO$_2$ for the CNP models (blue=positive, red=negative).** (a), Mean annual change in

462 standing leaf, fine root and wood C over 15 years, increasing across models from left to right

463 in g C m^{-2} yr^{-1}. (b), The mean change in C allocation for fine roots and wood in %. (c), Mean

464 change in tissue stoichiometry in absolute terms in g C g P^{-1} and change in P use efficiency

465 over 15 years in g C g P^{-1} yr^{-1}. (d), Mean change in ecosystem P input and output (leaching)

466 fluxes in g P m^{-2} yr^{-1} and in final P stock in biomass, organic soil, mineral soil and total

467 ecosystem in g P m^{-2}. (e), Mean change in plant P acquisition processes, including net P

468 mineralization, biochemical P mineralization and P uptake in g P m^{-2} yr^{-1}, and secondary and

469 labile P pools in g P m^{-2}. For both, (d) and (e), P flux changes are differences of cumulative

470 fluxes after 15 years and P pool changes are differences in pools after 15 years.

471 **METHODS**

472 **Site description**

473 Model simulations were conducted at the AmazonFACE experimental site in Central

474 Amazonia (2º35'39" S, 60º12'29'' W). AmazonFACE is an integrated model-experiment

475 project that aims to assess the effects of high CO_2 concentrations on the ecology and

476 resilience of the Amazon rainforest (http://amazon-face.org/). The experiment is currently

477 being established and is situated in a *terra firme* forest on a plateau characterized by highly

478 weathered, deep, clay sediment soil (with a clay fraction of 76%), classified as a Geric

479 Ferrasol[45]. The site and the surrounding area have been subjected to various long-term

480 measurement activities[25,46–49], coordinated by the Large-Scale Biosphere-Atmosphere

481 Program (LBA; http://lba2.inpa.gov.br/) in Amazonia, including the "K34" eddy covariance

482 flux tower[26], located approximately 2 km away from AmazonFACE site. Mean annual

483 precipitation at K34 from January 2000 to December 2015 was 2600 mm yr^{-1}, and the mean

484 temperature was 26°C.

485 **Model descriptions**

486 Fourteen ecosystem models with contrasting representations of ecosystem functioning and

487 nutrient cycling were applied to the experiment (Extended Data Table 3). C cycle dynamics

488 without nutrient cycle feedbacks are represented in the "C-only" models (InLand, ED2 and

489 ELM-FATES)[50–52]; C and N dynamics are represented in the "CN" models (LPJ-GUESS, O-

490 CN, JULES, CABLE-POP(CN) and GDAY(CN))[53–55]; and C, N, and P dynamics are

491 represented in the "CNP" models (ELM-ECA, ELM-CTC, CABLE, CABLE-POP,

492 ORCHIDEE, and GDAY)[19–24]. Two models were included with a respective CN and CNP

493 version (GDAY and CABLE-POP) to directly assess the effect of considering P dynamics.

494 The other models were treated as a non-random sample from the possible C, CN, and CNP

495 modelling assumptions. Four of the models are dynamic vegetation models: CABLE-POP

496 considers dynamic establishment and mortality with fixed plant functional type (PFT)

497 composition, while LPJ-GUESS, ED2 and ELM-FATES also consider dynamic PFT

498 composition. Photosynthesis is based on formulations by Farquahar[56] or derivations thereof in

499 all of the models[57,58] (Extended Data Table 3).

500 Prognostic C allocation fractions are based on functional relationships among tissues, e.g.,

501 fixed ratios between sapwood and leaf area in CABLE-POP, LPJ-GUESS, ED2, GDAY,

502 ORCHIDEE, O-CN, JULES, and ELM-FATES, and on resource dependence, e.g., higher root

503 allocation under water or nutrient stress in LPJ-GUESS, ELM-ECA, GDAY, O-CN,

504 ORCHIDEE, ED2 and ELM-FATES. C allocation fractions are fixed in InLand and CABLE.

505 Nutrient limitation is determined by the difference between demand and supply (via root

506 uptake and resorption) of N or P, with the most limiting nutrient determining the degree of

507 limitation. The photosynthetic parameters V_{cmax} and/or J_{max} are controlled by leaf N in all CN

508 and CNP models except JULES, while leaf P additionally downregulates gross primary

509 productivity (GPP) in all CNP models except ORCHIDEE. N controls net primary

510 productivity (NPP) in some of the models, i.e., O-CN, JULES, ORCHIDEE, CABLE and

511 CABLE-POP, and additionally downregulates growth efficiency (GPP/LAI) in CABLE and

512 CABLE-POP.

513 Maintenance respiration is dependent on temperature in all models and is additionally

514 controlled by tissue N content in all of the models that consider the N cycle with the exception

515 of GDAY, where Ra is a fixed fraction of GPP. Plant tissue stoichiometry in the CN and CNP

516 models is either fixed (ELM-CTC and JULES) or varies within or without bounds (all other

517 models). The nutrient resorption rates in the CN and CNP models are always fixed fractions

518 of the nutrient content in leaves and roots. Competition for nutrients between plant uptake and

519 decomposition processes is handled differently. Nutritional demands for the decomposition

520 process (representing microbial demands) are met entirely first in some models (CABLE, O-

521 CN, ORCHIDEE, and GDAY), are based on relative demands between decomposition and

522 plant uptake (ELM-CTC), or are determined via a multiple consumer approach including

523 adsorption to mineral surfaces (ELM-ECA). Nutrient uptake is a function of plant demand and

524 nutrient availability in all models and is further controlled by a measure of root mass in LPJ-

525 GUESS, GDAY, ORCHIDEE, and O-CN.

526 Soil organic matter (SOM) decomposition is limited by soil mineral N availability in most CN

527 and CNP models (except O-CN and ORCHIDEE) and additionally by labile P availability in

528 most CNP models (except GDAY and ORCHIDEE). P in SOM can also be mineralized via

529 phosphatase, decoupling the P cycle from the C and N cycle, termed biochemical P

530 mineralization in the P models. Biochemical P mineralization is a function of the slow SOM

531 pool turnover in CABLE, CABLE-POP and GDAY, as well as substrate availability in

532 ORCHIDEE, ELM-ECA and ELM-CTC. Biochemical P mineralization is upregulated with

533 higher plant P stress, representing higher phosphate production (not specified if by plants or

534 microbes), in ELM-ECA, ELM-CTC and ORCHIDEE.

535 N inputs originate from N deposition (prescribed by model protocol) and N fixation

536 (prescribed individually). N fixation is either fixed, calculated empirically as a fraction of

537 NPP or evapotranspiration (GDAY, JULES, ORCHIDEE, ELM-CTC, LPJ-GUESS, CABLE,

538 and CABLE-POP), or based on an optimization scheme (ELM-ECA and O-CN). P inputs

539 originate from weathering (prescribed individually) and deposition (prescribed by model

540 protocol). Release of P from rock weathering is a fixed, soil type-specific rate in CABLE and

541 CABLE-POP, a function of the parent P pool in ELM-ECA, ELM-CTC, and GDAY or

542 described as a function of lithology, runoff and air temperature in ORCHIDEE. N and P

543 losses occur from leaching, modelled as a function of the size of the labile P and mineral N

544 pool, respectively, and additionally controlled by runoff in ELM-ECA and ORCHIDEE.

545   The number of inorganic P pools and their precise definition varies among the models. We

546   consider two inorganic P pools relevant for our analysis: the labile P pool and the secondary P

547   pool. The labile P pool encompasses plant-available inorganic P, represented in most CNP

548   models by two separate pools connected by sorption dynamics and effectively in equilibrium

549   (described by Langmuir dynamics in most models and a linear approach in ORCHIDEE). The

550   labile P pools follow different nomenclature in the models but are comparable in

551   functionality: the P in soil solution (called labile or solution P) is readily available to plants in

552   the model time step, while the non-dissolved P (referred to as sorbed or sorbed labile P pool)

553   can become available to plants on yearly to decadal time scales due to desorption. The

554   secondary P pool represents P strongly sorbed by minerals, which is largely unavailable but

555   may enter the labile P pool on centennial time scales and, depending on model assumptions,

556   may be driven by plant P stress.

557   **Model simulations**

558   Models were forced with 16 years of observed local meteorology (2000 to 2015) from the

559   K34 flux tower[26]. Meteorological data from July 1999 to December 2015 of near-surface air

560   temperature, rainfall, downward shortwave radiation, downward longwave radiation, vapour

561   pressure deficit, surface pressure, relative humidity, and wind speed were available for model

562   input. Specific humidity was calculated based on observed relative humidity and surface

563   pressure. All data time series were subject to quality control (i.e., removal of outliers) and gap

564   filling using the variables' climatological mean. Precipitation data gaps were filled from a

565   nearby weather station of the Tropical Rainfall Measuring Mission network.

566   Simulations are initialized with a spin-up routine resulting in equilibrium conditions of C

567   stocks (and N, and P, if applicable) representing the year 1850. The 16-year meteorological

568   time series are continuously repeated throughout the whole spin-up, during the transient phase

569   (1851 to 1998), and during our model-experiment phase (1999 to 2013), representative of a

570   15-year long AmazonFACE experiment. Global datasets are used as inputs for atmospheric

571   CO_2[59,60], N deposition[61,62], and P deposition[63]. Atmospheric CO_2, N and P deposition levels

572   were set to 284.7 ppm, 1.43 kg N ha^{-1} yr^{-1}, and 0.144 kg P ha^{-1} yr^{-1} in 1850, respectively, and

573   follow historical changes during the transient and model experiment phase.

574   Other site parameters used for parameterization of the models are derived from *in situ*

575   measurements and include rooting and soil depth (set to rooting depth), soil hydraulic

576   parameters, specific leaf area (SLA), and soil texture (Extended Data Table 2). Soil hydraulic

577   parameters are derived from pedotransfer functions[64] and site-specific measurements of soil

578   properties[65]. Soil hydraulic parameters were included in models that accounted for this

579   functionality to allow for a better representation of soil water dynamics in tropical soils

580   (Extended Data Table 2).

581   Two model experiments are performed over the 15-year long experiment phase by each model

582   to assess the effect of elevated CO_2: 1) the ambient run (AMB) and 2) the elevated CO_2 run

583   (ELE). In the AMB run, the atmospheric CO_2 is set to ambient levels and is employed for

584   model evaluation against *in situ* measurements, including C fluxes from the K34 flux tower.

585   The ELE run represents the planned AmazonFACE experiment with a step change increase of

586   200 ppm at the start of the model experiment and continuous tracking of CO_2 levels in AMB

587   plus 200 ppm thereafter. Model outputs are analysed in biological years of seasonality (July to

588   June), and the difference between the elevated CO_2 run and the control run are used to infer

589   the model-based CO_2 effect.

590   **Model output analysis**

591   The analysis of the modelled output includes the evaluation of modelled ambient conditions

592   relative to *in situ* observations and hypotheses-based analyses of the modelled CO_2 responses.

593   We employ a structural analysis of the model simulations[9,66–68], splitting model outcomes into

594   the underlying processes to identify crucial model assumptions determining diverging

595   predictions for the FACE experiment. We focus on the simulated increase in biomass C due to

596   eCO_2 and the underlying nutrient control thereon.

597   Biomass C dynamics are a result of primary productivity, C allocation and turnover. We first

598   analyse the effect of eCO_2 on gross primary productivity (GPP), net primary productivity

599   (NPP), autotrophic respiration (Ra), and the resulting plant carbon use efficiency (CUE),

600   where CUE = NPP/GPP. We then assess changes in NPP allocation fractions to biomass

601   compartments of wood, fine roots and leaves, and the resulting effect on biomass C turnover

602   in response to eCO_2. Specific tissue turnover rates are fixed in all models, but overall biomass

603   C turnover changes as a result of changing C allocation to tissue compartments. Turnover

604   rates of biomass C pools are calculated as the fraction of total litter fall per total biomass pool

605   size (Extended Data Table 4).

606   Plant nutrient cycle feedbacks to eCO_2 are assessed by splitting the responses into plant N

607   uptake (NUP) and plant N use efficiency (NUE), where NUE = NPP/NUP, and similarly into

608   P uptake (PUP) and P use efficiency (PUE), where PUE = NPP/PUP. The responses of NUE

609   and PUE to eCO_2 are further split into changes in tissue C allocation (differing in C:N and

610   N:P ratios) and changes in tissue stoichiometry (flexible C:N and N:P ratios). Soil nutrient

611   cycle feedbacks to eCO_2 are determined by separating eCO_2 responses in N and P

612   mineralization rates (N and P mineralization from microbial decomposition of SOM and

613   biochemical P mineralization of organic P via phosphatase) and the balance of ecosystem N

614   and P inputs (N fixation, N and P deposition, and P weathering) and losses (N and P

615   leaching).

616   **Data availability**

617   Model output data used for analyses and figures have been archived in a GitHub repository

618   (https://github.com/Kaaze7/AmzFACE-model-ensemble-2019).

619   **Code availability**

620   Code used for analyses and figures have been archived in a GitHub repository

621   (https://github.com/Kaaze7/AmzFACE-model-ensemble-2019).

REFERENCES METHODS

45. Quesada, C. A. *et al.* Variations in chemical and physical properties of Amazon forest soils in relation to their genesis. *Biogeosciences* **7,** 1515–1541 (2010).

46. Chambers, J. Q. *et al.* Respiration from a Tropical Forest Ecosystem : Partitioning of Sources and Low Carbon Use Efficiency. *Ecol. Appl.* **14,** 72–88 (2004).

47. Aragão, L. E. O. C. *et al.* Above- and below-ground net primary productivity across ten Amazonian forests on contrasting soils. *Biogeosciences* **6,** 2759–2778 (2009).

48. Holm, J. A., Chambers, J. Q., Collins, W. D. & Higuchi, N. Forest response to increased disturbance in the central Amazon and comparison to western Amazonian forests. *Biogeosciences* **11,** 5773–5794 (2014).

49. Hadlich, H. L. *et al.* Recognizing Amazonian tree species in the field using bark tissues spectra. *For. Ecol. Manage.* **427,** 296–304 (2018).

50. Kucharik, C. J. *et al.* Testing the performance of a dynamic global ecosystem model: Water balance, carbon balance, and vegetation structure. *Global Biogeochem. Cycles* **14,** 795–825 (2000).

51. Fisher, R. A. *et al.* Taking off the training wheels: The properties of a dynamic vegetation model without climate envelopes, CLM4.5(ED). *Geosci. Model Dev.* **8,** 3593–3619 (2015).

52. Medvigy, D., Wofsy, S. C., Munger, J. W., Hollinger, D. Y. & Moorcroft, P. R. Mechanistic scaling of ecosystem function and dynamics in space and time: Ecosystem Demography model version 2. *J. Geophys. Res. Biogeosciences* **114,** (2009).

53. Smith, B. *et al.* Implications of incorporating N cycling and N limitations on primary production in an individual-based dynamic vegetation model. *Biogeosciences* **11,** 2027–2054 (2014).

54. Zaehle, S. & Friend, A. D. Carbon and nitrogen cycle dynamics in the O-CN land

647   surface model: 1. Model description, site-scale evaluation, and sensitivity to parameter

648   estimates. *Global Biogeochem. Cycles* **24,** n/a-n/a (2010).

649 55. Best, M. J. *et al.* The Joint UK Land Environment Simulator (JULES), model

650   description – Part 1: Energy and water fluxes. *Geosci. Model Dev.* **4,** 677–699 (2011).

651 56. Farquhar, G. D., von Caemmerer, S. & Berry, J. A. A biochemical model of

652   photosynthetic CO2 assimilation in leaves of C3 species. *Planta* **149,** 78–90 (1980).

653 57. Collatz, G. J., Ball, J. T., Grivet, C. & Berry, J. A. Physiological and Environmental-

654   Regulation of Stomatal Conductance, Photosynthesis and Transpiration - a Model That

655   Includes a Laminar Boundary-Layer. *Agric. For. Meteorol.* **54,** 107–136 (1991).

656 58. Kull, O. & Kruijt, B. Leaf photosynthetic light response: A mechanistic model for

657   scaling photosynthesis to leaves and canopies. *Funct. Ecol.* **12,** 767–777 (1998).

658 59. Etheridge, D. M. *et al.* Natural and anthropogenic changes in atmospheric CO2over the

659   last 1000 years from air in Antarctic ice and firn. *J. Geophys. Res. Atmos.* **101,** 4115–

660   4128 (1996).

661 60. MacFarling Meure, C. *et al.* Law Dome CO $_2$, CH $_4$ and N $_2$ O ice core records

662   extended to 2000 years BP. *Geophys. Res. Lett.* **33,** L14810 (2006).

663 61. Lamarque, J. F. *et al.* Historical (1850-2000) gridded anthropogenic and biomass

664   burning emissions of reactive gases and aerosols: Methodology and application. *Atmos.*

665   *Chem. Phys.* **10,** 7017–7039 (2010).

666 62. Lamarque, J. F. *et al.* Global and regional evolution of short-lived radiatively-active

667   gases and aerosols in the Representative Concentration Pathways. *Clim. Change* **109,**

668   191–212 (2011).

669 63. Wang, R. *et al.* Global forest carbon uptake due to nitrogen and phosphorus deposition

670   from 1850 to 2100. *Glob. Chang. Biol.* **23,** 4854–4872 (2017).

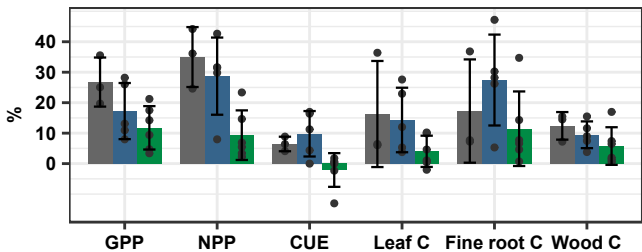671 64. Tomasella, J. & Hodnett, M. Pedotransfer functions for tropical soils. in *Developments*

672   *in Soil Science* **30,** 415–429 (Elsevier, 2004).

673 65. Marthews, T. R. *et al.* High-resolution hydraulic parameter maps for surface soils in

674   tropical South America. *Geosci. Model Dev.* **7,** 711–723 (2014).

675 66. De Kauwe, M. G. *et al.* Where does the carbon go? A model-data intercomparison of

676   vegetation carbon allocation and turnover processes at two temperate forest free-air

677   CO2enrichment sites. *New Phytol.* **203,** 883–899 (2014).

678 67. Walker, A. P. *et al.* Comprehensive ecosystem model   data synthesis using multiple

679   data sets at two temperate forest free   air CO2 enrichment experiments: Model

680   performance at ambient CO2 concentration. *J. Geophys. Res. Biogeosciences* **119,** 937–

681   964 (2014).

682 68. Medlyn, B. E. *et al.* Using ecosystem experiments to improve vegetation models. *Nat.*

683   *Clim. Chang.* **5,** 528–534 (2015).

684   Table 1. List of key processes and variables that need to be constrained by observational

685   estimates in order reduce uncertainty in P cycle control on the eCO_2 effect ecosystem models.

(H1) Plant C budget	Measurements needed
Canopy scale C assimilation	• Seasonal dynamics of leaf area and photosynthetic capacity • Photosynthetic acclimation
Plant tissue respiration	• Control of drought stress, nutrient limitation and P content • Wood and root respiration
Biomass growth	• Belowground biomass compartments • Long term growth rates
(H2) Plant P use	
Plant tissue C:P and N:P stoichiometry	• Plasticity versus adaptability to (experimental) change in eCO_2 or nutrient availability • Functionality of tissue P • Wood P content /stoichiometry
Plant tissue P resorption	• P content in live tissue and fresh litter • Plasticity versus adaptability to (experimental) change in eCO_2 or nutrient availability
(H3) Plant P acquisition	
P desorption due to plant exudation	• Interactions with microorganisms (directly or via microorganisms) • Cost of exudation vs. plant P uptake
P acquisition due to fine root production	• Surface litter activity • Fine root allocation fractions • Fine root productivity vs. plant P uptake
Biochemical P mineralization (via phosphatase)	• Phosphatase activity and relation to P mineralization • Plant production of phosphatase vs. plant-induced production by microorganisms • Cost of phosphatase production vs. plant P acquisition
Other interactions	
Plant N availability	• Ecosystem N budget • Symbiotic and free-living N fixation • Control of N availability on P acquisition
Plant water availability	• Control on P mineralization and transport dynamics • Control on of water and P limitation on eCO_2 effect

686
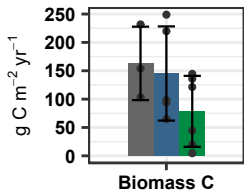
a Final response

b Initial response
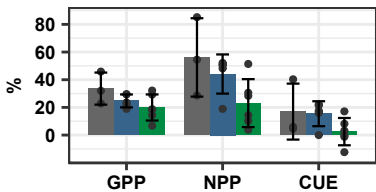
c Final response

C models   CN models   CNP models

Control of phosphorus feedbacks on the biomass carbon response to eCO₂

Legend: None, Intermediate, High

Process flow (left diagram): Photosynthesis; Maintenance respiration; Leaf N:P; P resorption; Leaf turnover; Biomass growth; Carbon allocation; Wood N:P; Desorption inorg. P; Biochemical mineralization org. P; Litter decomposition; P uptake; Litter N:P; SOM decomposition; SOM N:P

Models: CABLE, CABLE-POP, G'DAY, ELM-CTC, ELM-ECA, ORCHIDEE

a Biomass C gain

C leaf, C fine root, C wood (g C m^{-2} yr^{-1})

b C allocation fraction

Fine roots, Wood (%)

c Plant stoichiometry and P use efficiency

Leaf C:P, Biomass C:P, Litter C:P, PUE (g C g P^{-1} yr^{-1})

d P ecosystem retention

P input, P leaching, P biomass, P organic soil, P mineral soil, P ecosystem (g P m^{-2} yr^{-1})

e P plant acquisition

P net min., P bioch. min., P secondary, P labile, P uptake (g P m^{-2} yr^{-1})